Journal of Wind Engineering & Industrial Aerodynamics 202 (2020) 104192

Contents lists available at ScienceDirect

Journal of Wind Engineering & Industrial Aerodynamics

journal homepage: www.elsevier.com/locate/jweia

The significant impact of ribs and small-scale roughness on cylinder drag crisis

Arne Kilvik Skeide [a], Lars Morten Bardal [b], Luca Oggiano [a,b], R. Jason Hearst [a,*]

[a] Department of Energy & Process Engineering, Norwegian University of Science & Technology, NO-7491, Trondheim, Norway
[b] Centre for Sports Facilities & Technology, Norwegian University of Science & Technology, NO-7491, Trondheim, Norway

ARTICLE INFO

Keywords:
Drag
Cylinder
Ribs
Roughness
Drag crisis

ABSTRACT

The impact of flow-normal ribs and small-scale surface roughness on the drag and vortex shedding of a circular cylinder was investigated. Three rib heights, four relative rib spacings and three different forms of micro-roughness were combined to produce 28 unique surface coatings for the cylinder. The drag was measured in a wind tunnel for Reynolds numbers in the range $20,000 < Re < 160,000$, representing nearly a decade change centred about the drag crisis. The drag measurements were complemented by hot-wire measurements in the wake to investigate the vortex shedding frequency. The results show significant average drag reduction, up to 23%, for most of the ribbed geometries compared to a smooth cylinder for $Re < 160,000$. Increasing the rib height was found to reduce the critical Reynolds number and increase the minimum drag coefficient. Varying the rib spacing resulted in an "optimal" spacing, approximately five times the rib height, that caused the lowest critical Reynolds number. Increasing the micro-roughness resulted in a reduction in the critical Reynolds number and an increase in the minimum drag coefficient.

1. Introduction

The flow around circular cylinders and the resulting forces have been studied extensively over the last century. This is largely due to the fact that this fundamental flow has far-reaching applications. Flow around circular cylinders can, for instance, be found around wind turbine towers, tall buildings, oil platforms and in sports aerodynamics. These are applications where the resulting forces have significant impact on performance and design. It is therefore crucial to find ways to reduce these forces.

The drag, F_D, is of principal interest in many applications and is typically non-dimensionalised as the drag coefficient,

$$C_D = \frac{F_D}{\frac{1}{2}\rho U^2 A}, \tag{1}$$

where ρ is the fluid density, U is the free-stream velocity and A is the frontal area. As a first order approximation, C_D is a function of the shape, the motion and the surface of the cylinder (Oggiano et al., 2013), i.e., $C_D = f(\text{shape, motion, surface})$. The shape and motion are dependent on the form of the cylinder and the Reynolds number,

$$Re = \frac{Ud}{\nu}, \tag{2}$$

where d is the characteristic length, i.e., the diameter for spheres and cylinders, and ν is the kinematic viscosity of the fluid. The dependence of C_D of a circular cylinder on Re, known as the C_D-Re curve, is well-documented across a wide Re range. Roshko (1961), Schewe (1983, 2001) and Achenbach (1971), among others, have shown that the C_D-Re curve can be roughly divided into four flow regimes: the subcritical, critical, supercritical and transcritical regimes. The so-called 'drag crisis', a sudden reduction in drag relative to the change in Re, identifies the critical regime, with the subcritical (low Re) and supercritical (high Re) regimes flanking either side of the drag crisis. The transcritical regime occurs at very high Re, where there is a return to organised vortex shedding (Roshko, 1961; Schewe, 1983), but this regime is not the focus herein. By changing the surface roughness of the cylinder, the Reynolds number range of each of these regimes will also change (Roshko, 1961; Achenbach, 1971). Changing the surface roughness yields a different critical Reynolds number, Re_c, defined as the Re at the end of the critical flow regime and a different minimum C_D ($C_{D,min}$). Schewe (2001) analysed the drag of a smooth cylinder and found the subcritical C_D to be between 1.1 and 1.2, Re_c to be approximately 300 000, and $C_{D,min}$ to be

* Corresponding author.
E-mail address: jason.hearst@ntnu.no (R.J. Hearst).

https://doi.org/10.1016/j.jweia.2020.104192
Received 12 November 2019; Received in revised form 29 February 2020; Accepted 5 April 2020
Available online xxxx

approximately 0.2. This means that a smooth cylinder will experience a sudden decrease in drag for $Re > 300,000$. However, many applications do not reach this Re. For instance, the arms of a cyclist, if modelled as a cylinder, would experience flow in the range $25,000 < Re < 100,000$. Thus, if one wishes to push the drag crisis to lower Re, some intervention must take place.

A great deal of research has been done on engineering surface structures which could manipulate the flow around bodies, causing the lowest possible drag forces in a given Re range. Because drag reduction is closely related to energy savings, the applications are far-reaching. Some strategies include: surface roughness (Achenbach, 1971; Nakamura and Tomonari, 1982; Hsu et al., 2019), dimples (Bearman and Harvey, 1993), grooves (Kimura and Tsutahara, 1991; Yamagishi and Oki, 2004, 2005), riblets (Walsh and Weinstein, 1979; Ko et al., 1987; Lim and Lee, 2002), spanwise waviness (Ahmed and Bays-Muchmore, 1992; Lam and Lin, 2009), helices (Lee and Kim, 1997; Zhou et al., 2011), wake splitter plates (Roshko, 1961; Hwang and Yang, 2007), and spanwise ribs (Zdravkovich, 1981; Matsumura et al., 2002; Zhang et al., 2016).[1] The idea behind most of these methods is to induce turbulence in the boundary layer, thereby increasing the momentum of the flow, causing the flow to overcome the adverse pressure gradient and delay the separation from the cylinder. This would trigger the drag crisis and result in a narrower wake and a smaller drag coefficient.

One of these applications is the engineering of textiles for use in sports garments. Typically, different textiles result in changes to the roughness. Reducing the drag force has a large impact on the performance of athletes in many sports. Brownlie (1992) showed that athletes can be modelled as a system of bluff bodies; arms and legs as cylinders of different diameters for instance. Additionally, it has become quite common to see dimples or ribs on some athletic garments. This stems from riblets being shown to reduce the Re_c of a cylinder (Ko et al., 1987), and result in cylinder drag savings of up to 18.6% for $Re = 140,000$ (Lim and Lee, 2002).

Many methods have been used to parameterise surface roughness in simplified models. The idea behind creating these models is that knowledge of the surface geometry can lead to estimates of the drag force. While significant progress has been made, further development is still needed, c.f., Flack and Schultz (2010) and Flack (2018). Previous roughness studies have predominantly focused on zero-pressure-gradient flat plates, as this setup does not have the added complication of flow separation and pressure gradients. Nonetheless, these two problems are commonplace in engineering flows. Achenbach (1971) used a relative roughness model to describe the surface topology of a cylinder. This model relates the drag of a cylinder to Re and the relative roughness k_s/d, which is the ratio of the mean height of roughness of the cylinder to the cylinder diameter. The results are obtained from experiments using artificially roughened surfaces (usually by gluing sand grains of a known size onto the cylinder) (Cengel and Cimbala, 2014). More recently, a similar approach was taken by Hsu et al. (2019) who placed different textile fabrics over a circular cylinder to change the surface roughness. After the roughness is applied with one of these methods, the surface with unknown drag is scanned to find the relative roughness k_s/d, and compared to experiments of an artificially roughened surface with the same k_s/d, to find the equivalent drag. This is equivalent to using the Moody diagram for pipe flows (Cengel and Cimbala, 2014), and has been used with some success for circular cylinders as well (Achenbach, 1971; Hsu et al., 2019). This method is, however, limited when multiple roughness scales of different orders of magnitude are superimposed on one another (Oggiano et al., 2013). For example, if a cylinder has ribs that are an order of magnitude larger than the micro-roughness superimposed on top of the ribs, then unified parameterisations of the roughness, e.g., $S10z$ from the ISO 25178 standard used by Hsu et al. (2019), are strongly biased towards the ribs. This could thus result in numerous surfaces with effectively the same k_s/d but very different drag.

[1] The references provided here are meant to be exemplary, but not exhaustive.

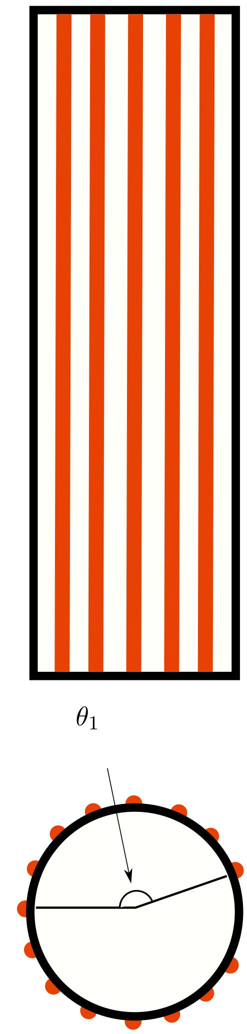

Fig. 1. Schematic of cylinder rib structure.

An example of this was shown by Bearman and Harvey (1993) using dimples on a cylinder.

An open question is how the aerodynamic properties (e.g., Re_c, $C_{D,min}$) vary with different rib geometries. Matsumura et al. (2002) tested three different cylinders with different numbers of equally distributed triangular ribs. They showed a tendency of lower Re_c with larger frequency of ribs, but more than three test cases would be needed to show a clear trend. The base of the ribs are also connected in the three cases, giving ribs of different shapes. It would be interesting to test the effect of ribs of equal shape, but different sizes and spacings. Zhang et al. (2016) did a numerical analysis on sinusoidal ribs, but only on one rib geometry and only on one subcritical Re. Semi-circular ribs would theoretically be a preferred choice since rounded bodies in general have a lower C_D than bodies with sharp edges. Another question that arises is what is the net effect of roughness of different scales? For instance, previous studies have focused on isolating rib-like structures from homogeneously distributed roughness. There has not been a dedicated study of the forces on a cylinder when both a rib structure (''macro-roughness'') and a homogeneous surface roughness (''micro-roughness'') are superimposed. Thus, how these surface treatments combine to create drag savings or excess is unknown.

This work investigates the aerodynamic properties of flow-normal, equally distributed, semi-circular ribs on a cylinder with superimposed micro-roughness. The size and spacing of the ribs are varied for three different micro roughness coatings. Correlations are then drawn between the surface topologies and the drag of the body.

Table 1
Surface coating parameter space. This table should be read as a list.

h mm	h/d	Δ mm	Δ/h	S	k_S^{max} mm
0.5	0.0067	2.5	2.5	A	0.10
1.0	0.0133	5.0	5.0	B	0.20
2.0	0.0267	10	10	C	0.42
		20	20		

2. Experimental set-up

2.1. Test cases

The present study investigates the drag and vortex shedding of a 417 mm long circular cylinder with a diameter of $d = 75$ mm. The diameter of the cylinder was chosen to achieve a range of Reynolds numbers that would capture the drag crisis for all test cases. The surface of the cylinder was altered between test cases by covering the cylinder with different textiles (hereafter referred to as surface coatings) whereupon the macro- and micro-surface topology were changed. The surface coatings consisted of two layers of fabric with 3D-printed ribs laminated in-between the two layers. The ribs had semicircular cross-sections, as illustrated in Fig. 1. Here, θ_1 is the angle between the front of the cylinder and the last rib. The value for θ_1 was between 150° and 160° for all surface coatings. A sector was left without ribs on the downstream side of the cylinder as a result of limitations in the manufacturing process. However, it was verified that separation always occurred well upstream of the last rib, and thus the impact of not having ribs on the leeward side of the cylinder was minimal.

The surface coatings were varied using three parameters: the relative height of the ribs (h/d, where h is the rib height), the relative spacing between the ribs (Δ/h, where Δ is the spacing between ribs), and maximum roughness height of the coating fabric (k_S^{max}); for simplicity the coating fabrics are referred to as A, B and C, in order of increasing roughness and their names are represented by the variable S. The different coating fabrics had different roughness resulting from different yarn and knit types. The parameter space spanned by the surface coatings is summarised in Table 1. This table should be read as a list, as it does not show explicit combinations of parameters. Instead, the combinations of parameters are represented by a naming convention for each surface coating given by $S_\alpha, h_\beta, \Delta_\gamma$, where α, β and γ indicate the coating fabric, rib height and rib spacing, respectively. For example, surface coating S_A, h_2, Δ_5 has coating fabric A with $k_S^{max} = 0.10$ mm, a rib height of $h = 2.0$ mm, and a rib spacing of $\Delta = 5.0$ mm. The parameters in Table 1 were combined into 28 unique surface coatings, which are detailed in Table 2. While theoretically, more combinations were possible, it was found that certain configurations either did not yield substantially different results or were too difficult to manufacture. Nonetheless, the present investigation represents the largest and most detailed parameter space explored for surface coating with both micro- and macroscopic roughness on a circular cylinder to date.

To verify the actual surface topology of the surface coatings, each coating was stretched onto a flat plate with the same perimeter as the test cylinder, and placed on a FESTO linear traverse under a MicroCAD premium surface scanner. A 73 mm × 10 mm (9119 pixel × 1236 pixel) area was scanned stitching together 6 frames with 7.7% overlap between adjacent scans. Surface scan examples are provided in Fig. 2.

2.2. Drag measurements

Drag measurements were performed in the small closed-circuit wind tunnel in the Fluid Mechanics Laboratory at the Norwegian University of Science and Technology. The wind tunnel test-section has a 1000 mm × 520 mm cross-section. Two 48 mm long dummy-cylinders with the same d as the test cylinder were placed between the test cylinder and the tunnel walls; an approximately 3 mm gap was left between the dummy cylinders and the test cylinder. This was done to minimise wind tunnel wall boundary layer effects. The frontal area of the test cylinder was used as the area, A, in equation (1). The aspect ratio of the cylinder in the present experiments is 5.56, which is similar to that in some previous studies (Roshko, 1961; Hsu et al., 2019) and is representative of aspect ratios that exist in many practical applications, e.g., human limbs. The nominal blockage of the cylinder in the test-section was 7.5%. Despite this being

Table 2
List of test cases with physical and aerodynamic properties.

Surface Coating	S	k_S^{max} [mm]	h [mm]	Δ[mm]	h/d	Δ/h	N_{ribs}	θ_1 [deg]	Re_c	$C_{D,min}$
S_A, h_0	A	0.10	0	–	0	–	0	–	–	–
$S_A, h_{0.5}, \Delta_5$	A	0.10	0.5	5.0	0.0067	10	35	157	123 000	0.53
$S_A, h_{0.5}, \Delta_{10}$	A	0.10	0.5	10	0.0067	20	19	152	107 000	0.51
$S_A, h_1, \Delta_{2.5}$	A	0.10	1.0	2.5	0.0133	2.5	46	156	87 000	0.52
S_A, h_1, Δ_5	A	0.10	1.0	5.0	0.0133	5	30	157	49 500	0.59
S_A, h_1, Δ_{10}	A	0.10	1.0	10	0.0133	10	18	157	43 000	0.61
S_A, h_1, Δ_{20}	A	0.10	1.0	20	0.0133	20	10	153	127 000	0.77
S_A, h_2, Δ_5	A	0.10	2.0	5.0	0.0267	2.5	23	154	43 000	0.63
S_A, h_2, Δ_{10}	A	0.10	2.0	10	0.0267	5	15	153	27 000	0.72
S_A, h_2, Δ_{20}	A	0.10	2.0	20	0.0267	10	9	150	31 000	0.80
S_B, h_0	B	0.20	0	–	0	–	–	–	138 500	0.49
$S_B, h_{0.5}, \Delta_{10}$	B	0.20	0.5	10	0.0067	20	19	152	97 000	0.52
$S_B, h_1, \Delta_{2.5}$	B	0.20	1.0	2.5	0.0133	2.5	46	156	83 000	0.52
S_B, h_1, Δ_5	B	0.20	1.0	5.0	0.0133	5	30	157	–	0.65
S_B, h_1, Δ_{10}	B	0.20	1.0	10	0.0133	10	18	157	88 500	0.54
S_B, h_1, Δ_{20}	B	0.20	1.0	20	0.0133	20	10	153	101 000	0.69
S_B, h_2, Δ_5	B	0.20	2.0	5.0	0.0267	2.5	23	154	73 000	0.59
S_B, h_2, Δ_{10}	B	0.20	2.0	10	0.0267	5	15	153	29 000	0.72
S_B, h_2, Δ_{20}	B	0.20	2.0	20	0.0267	10	9	150	33 000	0.96
S_C, h_0	C	0.42	0	–	0	–	–	–	57 000	0.61
$S_C, h_{0.5}, \Delta_{10}$	C	0.42	0.5	10	0.0067	20	19	152	75 000	0.57
$S_C, h_1, \Delta_{2.5}$	C	0.42	1.0	2.5	0.0133	2.5	46	156	49 000	0.68
S_C, h_1, Δ_5	C	0.42	1.0	5.0	0.0133	5	30	157	43 000	0.72
S_C, h_1, Δ_{10}	C	0.W42	1.0	10	0.0133	10	18	157	39 000	0.65
S_C, h_1, Δ_{20}	C	0.42	1.0	20	0.0133	20	10	153	–	0.75
S_C, h_2, Δ_5	C	0.42	2.0	5.0	0.0267	2.5	23	154	35 000	0.74
S_C, h_2, Δ_{10}	C	0.42	2.0	10	0.0267	5	15	153	$< 20\,000$	–
S_C, h_2, Δ_{20}	C	0.42	2.0	20	0.0267	10	9	150	59 000	1.16

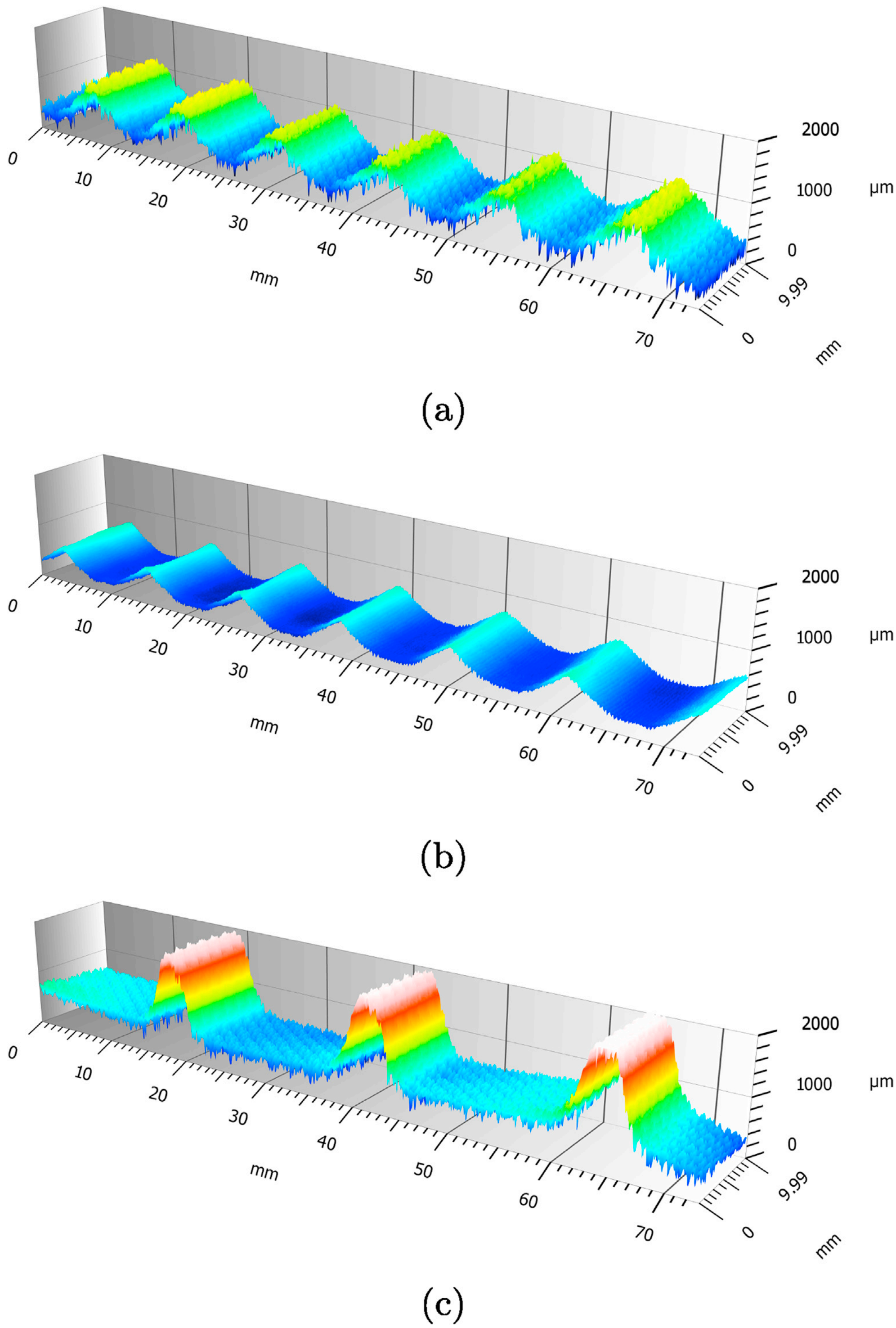

Fig. 2. 3-dimensional surface scans of surface coatings (a) S_C, h_1, Δ_{10}, (b) S_A, h_1, Δ_{10}, and (c) S_C, h_2, Δ_{20}.

slightly above the 6% recommendation of West and Apelt (1982), no blockage corrections were employed as the uncertainty induced by the correction arithmetic is of the same order as the possible blockage effects. As such, the results should be considered relative to each other rather than absolute. The test cylinder was connected to two AMTI MC3A-100 force sensors through a steel rod. Each sensor was connected to an AMTI GEN5 Smart Amp load cell amplifier, which in turn was connected to a computer running LabView. The drift in the signal was measured and calculated to be less then 1%. The wind tunnel setup is illustrated in Fig. 3.

In the present study, drag is measured through a dynamic scan rather than at individual velocity points. Each scan begins at $Re \approx 20,000$ and the velocity is increased steadily to approximately $Re \approx 160,000$ over a period of 4 min, while measuring at a frequency of 1000 Hz; over this range, the wind tunnel has a nominal background turbulence intensity of 0.7%. The Reynolds number scan procedure was repeated five times for each surface coating, giving five independent C_D-Re curves. These five curves were then averaged to yield a single continuous curve for each surface coating. This approach was used in place of independent static measurements so that the drag crisis could be identified more readily,

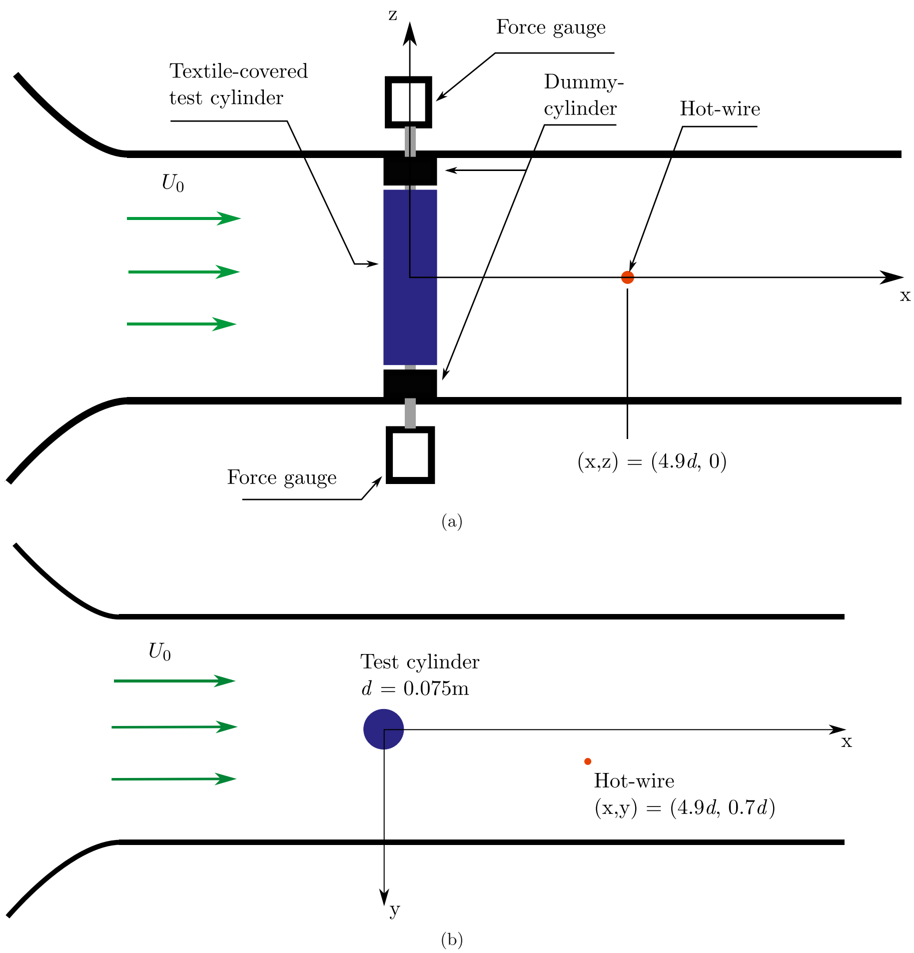

Fig. 3. Schematic of the wind tunnel setup including the position of the hot-wire. Both a (a) side view and (b) top view are provided. The schematic is not to scale.

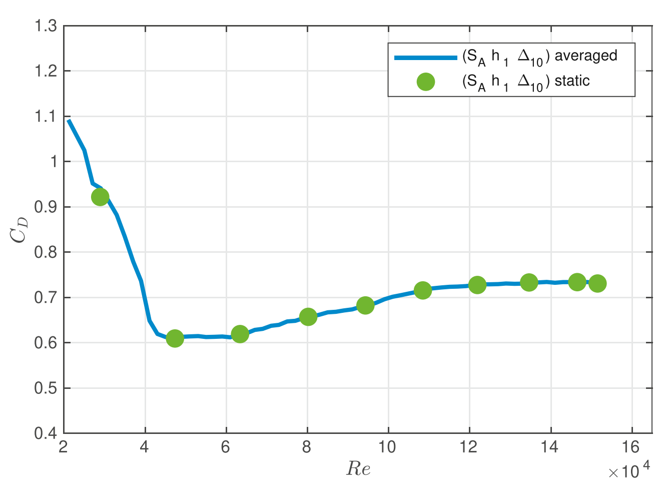

Fig. 4. Comparison of the averaged dynamic drag measurements with static drag measurements for S_A, h_1, Δ_{10}.

yielding more accurate values for Re_c and $C_{D,min}$. Nonetheless, static force measurements at constant Re were also performed for several surface coatings to verify that the dynamic measurement method was not a source of error. A representative comparison of the dynamic and static force measurements is provided in Fig. 4 where it can be seen that the two approaches are in good agreement.

2.3. Hot-wire anemometry

Velocity measurements in the wake of the cylinder were conducted in a separate experiment with a single-wire hot-wire (Dantec type 55P11) placed 4.9d downstream from the cylinder axis, 0.7d off the cylinder centerline and in the centre of the vertical axis. This position is the same as that used in the seminal work by Roshko (1961). The wires were operated in constant temperature mode with an overheat of 1.8 using a Dantec Streamline Pro anemometer. A pitot-static tube was placed 100 mm above and 20 mm downstream of the hot-wire, and a Dantec resistance temperature detector (RTD) probe was placed 20 mm above and 150 mm downstream of the hot-wire. Another pitot-static tube was placed 2 m upstream of the cylinder axis and at the centerline. The downstream pitot-static tube was used for the calibration of the hot-wire, while the upstream pitot-static tube measured the free-stream velocity. These were connected to a pressure transducer, and all signals were acquired using a National Instruments NI cDAQ-9174 (DAQ). The hot-wire and temperature outputs from the anemometer along with the pressure transducer were connected to a NI 9215 module in the DAQ.

The hot-wire was calibrated with 11 velocities fit with a fourth-order polynomial. Pre- and post-calibrations were performed at the start and end of each day of measurements to account for electrical drift. To correct for temperature drift, the methodology of Hultmark and Smits (2010) was employed. To assess the shedding phenomena in the wake of the cylinder, six velocities were sampled for each surface coating. The sampling time was 4 min for all cases, with a sample frequency of 75 kHz. An analog cut-off filter was set to 30 kHz. Turbulence spectra for two of the cases are shown in Fig. 5. The Strouhal numbers,

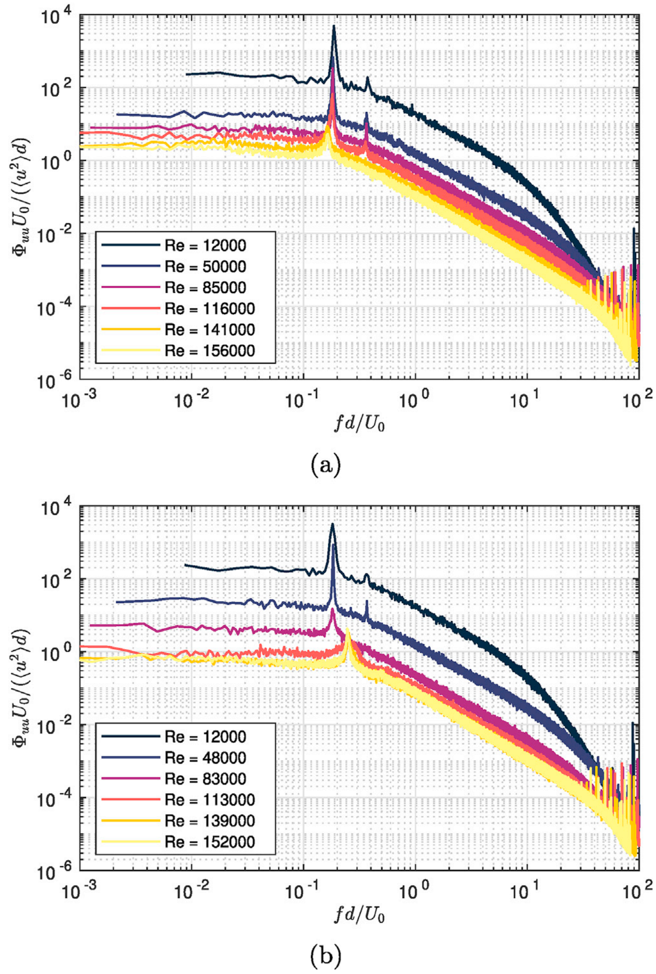

Fig. 5. Longitudinal velocity spectra for (a) the smooth cylinder and (b) S_A, $h_{0.5}$, Δ_{10}.

$$St = \frac{f_{\text{shed}} d}{U_0} \tag{3}$$

where f_{shed} is the shedding frequency, for each case were drawn from the spectra using the frequency from the distinct vortex shedding peaks.

3. Parametric study results and discussion

In order to gain an understanding of how the alterations to the surface coatings influence the drag and vortex shedding of the cylinder, we break the analysis down to study the effects of rib spacing, rib height, and surface micro-roughness separately. These are each investigated in the subsequent subsections. In general, specific subsets of test-cases with comparable parameters are identified and the C_D-Re curve is presented alongside the St-Re curve for each set of test cases. The discussion primarily focuses on how the critical Reynolds number (Re_c) and the minimum coefficient of drag ($C_{D,min}$) are impacted by the changes in surface topology. This investigation includes measurements of 28 different test cases. As such, results for each case are contained in the tables and the final summary figures of section 4. However, for brevity, detailed results are only presented for a few representative cases in this section.

3.1. Effect of rib spacing

Fig. 6 shows the Re-dependence of surface coatings with top fabric A, rib height 1.0 mm ($h/d = 0.0133$) and relative rib spacings in the range $2.5 \le \Delta/h \le 20$. The smooth cylinder case is provided as a benchmark. It

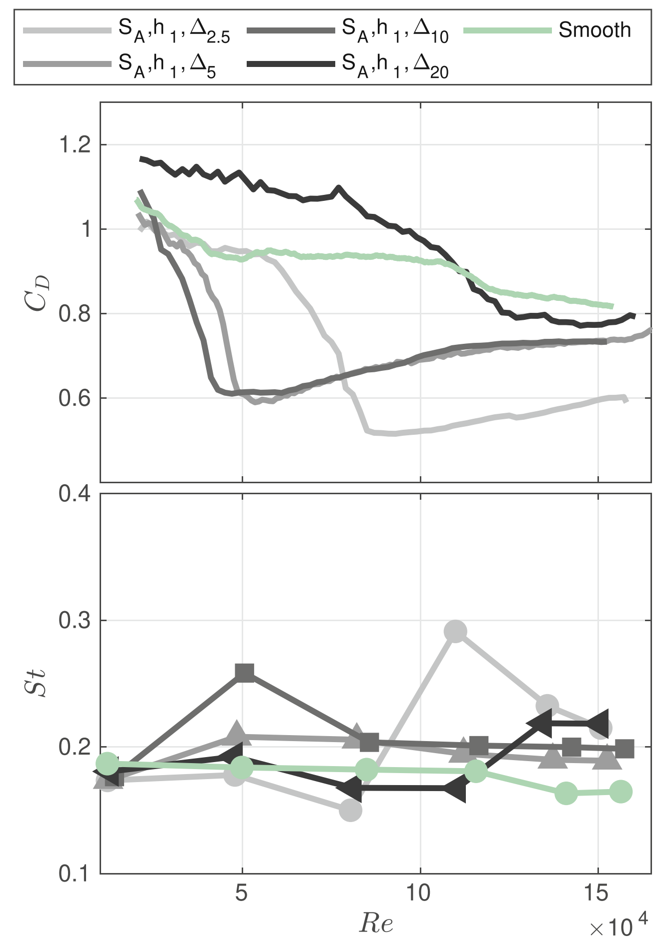

Fig. 6. Effect on C_D-Re curve by varying the rib spacing, for coating fabric A and $h/d = 0.0133$.

is significant to note that this first example illustrates that changing Δ/h has an impact on when drag crisis occurs, what the minimum drag achieved during drag crisis is, and the frequency of the dominant vortex shedding in the wake. In particular, for the cases shown in Fig. 6, the relative rib spacing $\Delta/h = 10$ (i.e., test case S_A, h_1, Δ_{10}) gave the lowest Re_c. However, $\Delta/h = 2.5$ ($S_A, h_1, \Delta_{2.5}$) gave the lowest $C_{D,min}$. Thus, these two parameters are impacted in different ways by Δ/h. The case with the largest spacing, $\Delta/h = 20$ (S_A, h_1, Δ_{20}), gave both the largest Re_c and $C_{D,min}$, suggesting that larger spacings have detrimental effects. There is thus a trend where increasing Δ/h increases $C_{D,min}$, and decreases Re_c until a critical spacing where the Re_c starts to increase again; passed this critical spacing, it would suggest that the addition of the ribs acts more to increase surface area than to reduce drag. This trend suggests there is a rib spacing that would give the lowest Re_c, and that this lies between $\Delta/h = 10$ and 20 for the cases presented in Fig. 6 with micro-roughness A.

The dependence of St on Re is plotted for the same cases in the bottom half of Fig. 6. This figure essentially shows how the shedding frequency changes with increasing Reynolds number for the different cases. In these curves, there are peaks at, or near, Re_c for the $\Delta/h = 2.5$, 10 and 20 cases. For $\Delta/h = 5$ (S_A, h_1, Δ_5), a peak at the critical Reynolds number is not visible. This is likely a result of it lying between the hot-wire test points, and thus the peak may have been missed. The general trend appears to be that St is relatively constant until drag crisis is reached, at which point the shedding frequency grows rapidly, before settling back to a supercritical state that resembles the subcritical state (within the Re-range investigated here). For high enough Re one would expect coherent cylinder shedding to disappear completely, but this is beyond the Re investigated herein (Anderson, 2017). The smooth cylinder measured in

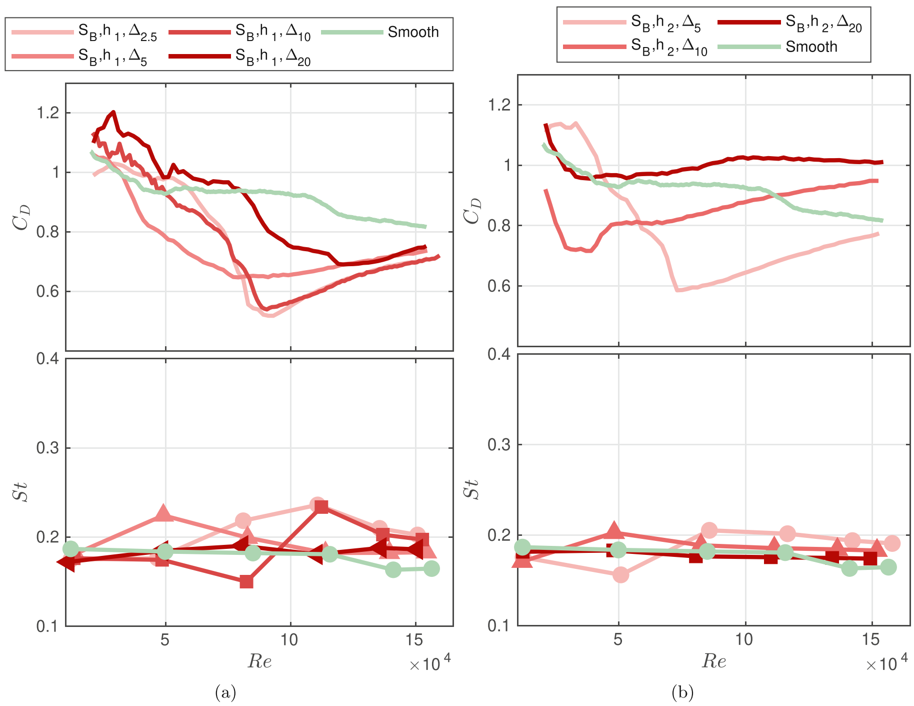

Fig. 7. Effect on C_D-Re curve and St by varying the rib spacing Δ, for coating fabric B and relative rib height (a) 0.0133 and (b) 0.0267.

this case is subcritical throughout the entire Re range, but the curves are consistent with the results obtained by Schewe (2001) for a smooth cylinder.

The results drawn from Fig. 6 are for a specific h with a specific micro-roughness, and changing spacing. To investigate the robustness of the results, we look at different h and micro-roughness configuration, but again change the spacing. For ribs with $h = 2.0$ mm ($h/d = 0.0267$) and the same coating fabric, the same general trends are observed; these results are not shown for brevity, and instead we focus on the next surface fabric (B) with $k_S^{max} = 0.20$ mm. In particular, Fig. 7(a) shows the results for fabric B with $h = 1.0$ mm ($h/d = 0.0133$) and $2.5 \leq \Delta/h \leq 20$. These C_D-Re curves do not show the exact same trend as seen for coating A. For coating B, $\Delta/h = 5$ (S_B, h_1, Δ_5) produces the lowest Re_c, while $\Delta/h = 10$ (S_B, h_1, Δ_{10}) and $\Delta/h = 2.5$ ($S_B, h_1, \Delta_{2.5}$) yield nearly identical results. Moreover, for $120,000 < Re < 160,000$, the curves for $\Delta/h = 5$ and 20 (S_B, h_1, Δ_5 and S_B, h_1, Δ_{20}) collapse; in fact, all four curves are quite similar in this region. This suggests that while the ribs may change Re_c, this micro-roughness may dominate the supercritical drag for ribs of this height. Similar St trends are apparent when compared to the smoother micro-roughness, but the overall variation in the shedding frequencies are diminished and the changes between the curves represent the changes in Re_c, as was also seen in Fig. 6.

Increasing the relative rib height to $h/d = 0.0267$ for micro-roughness B (Fig. 7(b)), and varying the rib spacing returns to the same trends observed for micro-roughness A (Fig. 6), i.e., there is a critical Δ/h that minimises Re_c before it grows again. The $C_{D,min}$ varies extensively for the three cases and increases for increasing spacing, yielding approximately $C_{D,min} = 0.6$, 0.7 and 0.95 for S_B, h_2, Δ_5, S_B, h_2, Δ_{10} and S_B, h_2, Δ_{20}, respectively. The variation in shedding frequency with Re, quantified as St in Fig. 7(b), results in peaks at Re_c, but these peaks are at lower St ($\lesssim 0.2$) compared to the those for micro-roughness A and $h/d = 0.0133$ (Fig. 6) and the one for the smooth cylinder (~ 0.4) shown by Schewe (2001). This supports the hypothesis that the frequency of the vortex shedding at Re_c is diminished by increasing micro-roughness. For $\Delta/h = 10$ (S_B, h_2, Δ_{20}), the St is relatively constant with Re. This indicates that the St-peak vanishes for large rib spacings and increasing rib height.

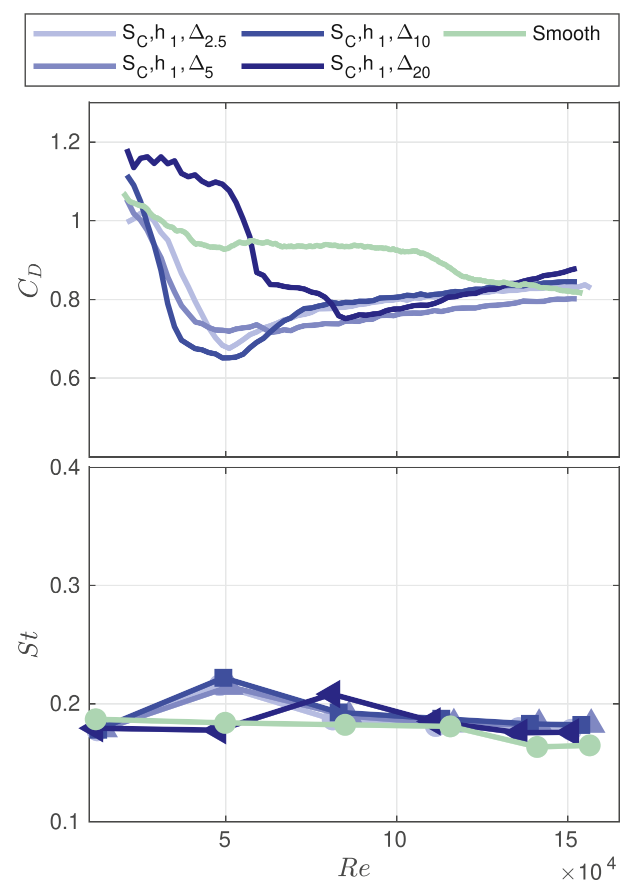

Fig. 8. Effect on C_D-Re curve and St by varying the rib spacing, for coating fabric C and relative rib height 0.0133.

Plotting results for micro-roughness C, $h/d = 0.0133$ and different rib spacings gives Fig. 8. The critical Reynolds numbers appear to roughly

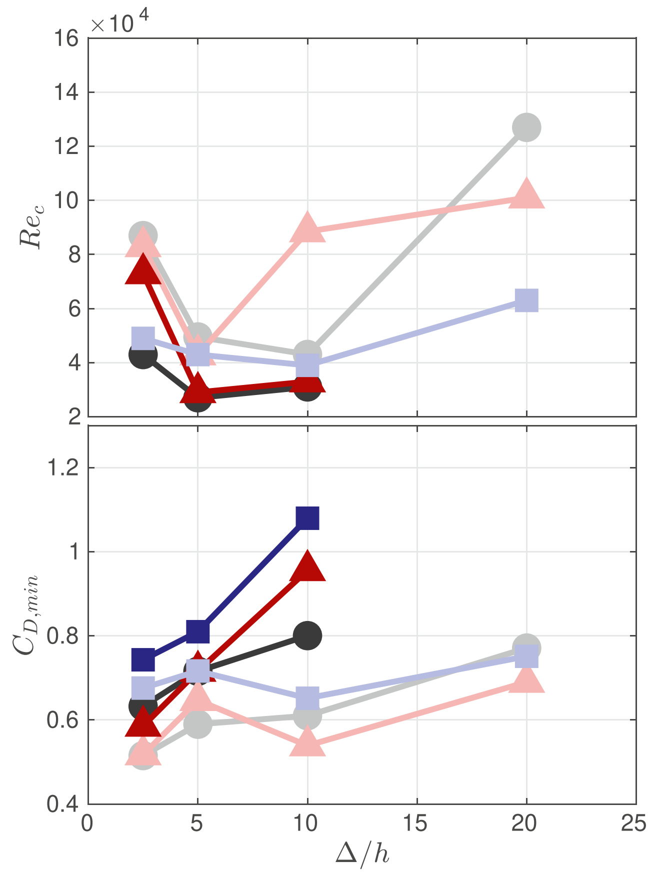

Fig. 9. The effect on Re_c and $C_{D,min}$ of varying the relative rib spacing. The different curves have different micro-roughness and h/d. Circles represent micro-roughness A, triangles represent B, and squares represent C. Darker colour identify larger rib height. (For interpretation of the references to colour in this figure legend, the reader is referred to the Web version of this article.)

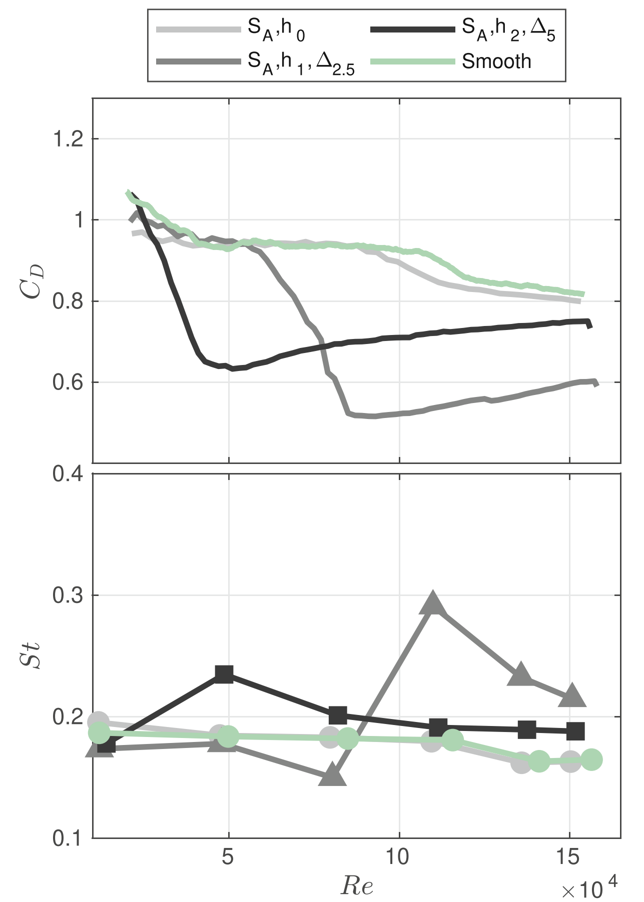

Fig. 10. Effect on the C_D-Re curve and the St by varying the relative rib height, for coating fabric A and relative rib spacing $\Delta/h = 2.5$.

follow the same trend as in Fig. 6, with decreasing Re_c from $\Delta/h = 2.5$ $(S_C, h_1, \Delta_{2.5})$ through $\Delta/h = 5$ (S_C, h_1, Δ_5) up to $\Delta/h = 10$ (S_C, h_1, Δ_{10}), before increasing again for $\Delta/h = 20$ (S_C, h_1, Δ_{20}). The variation between cases for the three smallest spacings are small compared to the changes for the other coatings (the maximum Re_c difference is 15 000), compared to a Re_c increase between S_C, h_1, Δ_{10} and S_C, h_1, Δ_{20} of approximately 50 000. $C_{D,min}$ is the smallest for S_C, h_1, Δ_{10} and largest for S_C, h_1, Δ_{20}, but the variations are small for this surface coating which is the roughest coating of the three. One can also notice that the curves for $S_C, h_1, \Delta_{2.5}$ and S_C, h_1, Δ_{10} collapse in the supercritical range, and the variations in C_D for the four curves are relatively small (approximately 0.05) for $80,000 < Re < 150,000$. This suggests again that the rougher micro-roughness dominates the supercritical regime, playing a more significant role there than the ribs.

From Fig. 8 one can see that the St curves for the three smallest rib spacings are approximately collapsed; they also have similar C_D-Re curves and hence Re_c. Once again the observation that there is a peak in St that corresponds to the location of Re_c and that the total variations in St are diminished for increasing micro-roughness are confirmed. Increasing the relative rib height to $h/d = 0.0267$ for micro-roughness C, yields the same trends as observed for other surface coatings and as such is not presented for brevity.

To summarise the effects of relative rib spacing (Δ/h), the present results suggest there is a Δ/h that minimises Re_c for the cylinder for each of the test cases. The Re_c results for all test cases are amalgamated in Fig. 9 where Re_c is explicitly plotted against Δ/h for each set of tests. In general, the spacing that results in the minimum Re_c appears to fall in the range $5 \leq \Delta/h \leq 10$. The increase in Re_c for $\Delta/h = 20$, which appears to exist across all cases, may be a result of the ribs acting to increase surface area rather than promote wake recovery. Moreover, cylinders with single ribs (Nebres and Batill, 1993) have been shown to be sensitive to the position of the rib relative to the incoming flow. It is possible this becomes a factor for higher rib spacings, but this topic is not investigated further here. Smaller spacings than the "optimal", appear to also result in adverse effects. When taken to the extreme, a spacing of $\Delta/h = 1$ would be perceived as a smooth cylinder and thus a return to the higher Re_c observed for the smooth case is consistent with the increase in Re_c and the decrease in $C_{D,min}$ (Fig. 9). Focusing on $C_{D,min}$, Δ/h appears to generally increase the minimum drag (Fig. 9). Thus, based on rib spacing alone, $\Delta/h = 5$ appears to optimise Re_c and it is generally desirable to keep the spacing small to maintain a low $C_{D,min}$.

3.2. Effect of rib height

The effect of rib height (h/d) is addressed in this section by comparing cases where it is the only parameter varied. In Fig. 10 cases with increasing h/d but constant micro-roughness (A) and relative spacing ($\Delta/h = 2.5$) are compared. Micro-roughness A without ribs (S_A, h_0) and the smooth cylinder are also plotted for reference. The smooth cylinder and S_A, h_0 are subcritical throughout the measured Re range, and thus those cases provide no information about its Re_c or $C_{D,min}$ other than that the drag crisis occurs at a higher Re. Comparing the curves, it appears $C_{D,min}$ increases and Re_c decreases for increasing h/d. Focusing on the shedding frequency (Fig. 10), S_A, h_0 and the smooth case do not show any peaks within the measured Re range suggesting they are always subcritical, while $S_A, h_1, \Delta_{2.5}$ and S_A, h_2, Δ_5 have peaks at their respective Re_c. The smaller rib height results in a shedding peak at a higher St. The

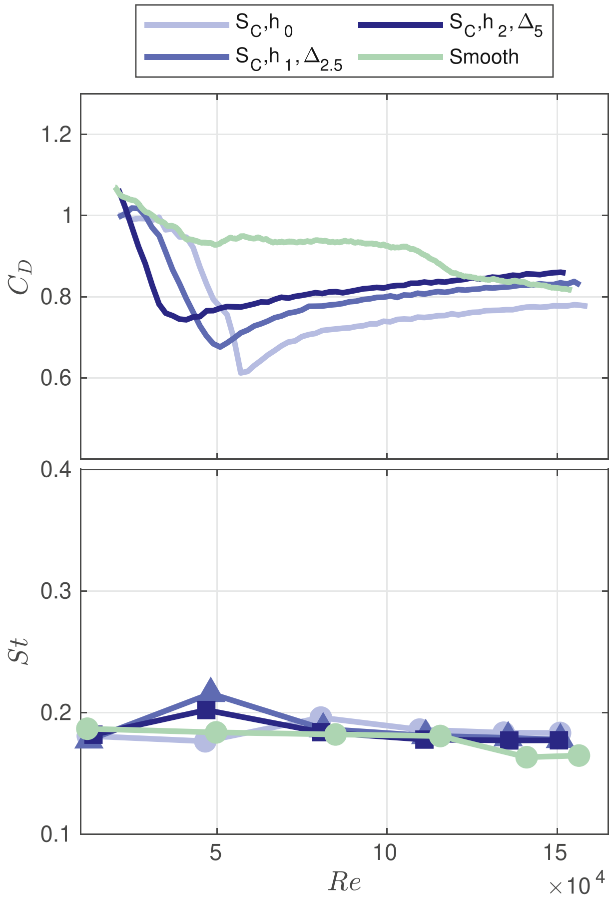

Fig. 11. Effect on the C_D-Re curve and the St by varying the relative rib height, for coating fabric C and relative rib spacing $\Delta/h = 2.5$.

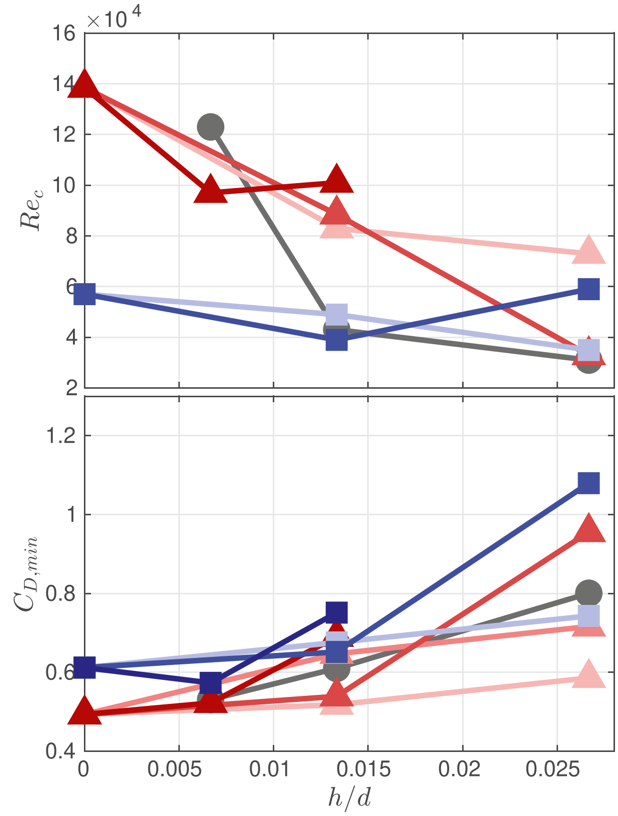

Fig. 12. The effect on Re_c and $C_{D,min}$ of varying the rib height. The different curves have different micro-roughness and Δ/h. Circles represent micro-roughness A, triangles represent B, and squares represent C. Darker colour identify larger Δ/h. (For interpretation of the references to colour in this figure legend, the reader is referred to the Web version of this article.)

same general trends are observed for the other rib spacings for both micro-roughness A and B (not shown for brevity).

The same general trends are also observed for the effect of rib size for various spacings with micro-roughness C, as illustrated in Fig. 11. It is of note though that the supercritical slope is similar for all cases and their supercritical C_D are also similar. Thus adding more evidence to the hypothesis that the supercritical region is dominated by the micro-roughness.

Summarising the general trends found in this section, increasing h/d for a given Δ/h and micro-roughness results in a decrease in Re_c, and an increase in $C_{D,min}$. These trends are clearly illustrated in Fig. 12, which shows global trends on $C_{D,min}$ and Re_c for increasing h/d.

3.3. Effect of surface coating

The previous results strongly suggest that the micro-roughness has an impact on drag crisis and the supercritical C_D curve. In this section, this idea is investigated further by comparing test cases where h/d and Δ/h are kept constant while the micro-roughness is changed. To get an initial impression of the general effect of changing the micro-roughness, consider Fig. 13. Here, three cases are shown for cylinders without ribs but with varying micro-roughness; the smooth cylinder is again provided as a benchmark. Fig. 13 shows that for the smoothest micro-roughness (S_A, h_0), the curve remains subcritical throughout the entire measurement range. As the micro-roughness is increased (S_B, h_0), the Re_c is reduced to approximately 140 000. Again, increasing the micro-roughness (S_C, h_0) decreases the Re_c further to approximately 60 000 while increasing the $C_{D,min}$ from roughly 0.5 to 0.6. This means that an increase in micro-roughness shifts the point of the $C_{D,min}$ to larger C_D and lower Re. This corresponds to what would be expected by the relative roughness model (Cengel and Cimbala, 2014). For the shedding frequency St, shown in Fig. 13, only S_B, h_0 shows an increase in the shedding frequency at the drag crisis, however, drag crisis does not occur within the tested Re-range for the smooth case and S_A, h_0 and the roughest micro-roughness case has consistently been shown in the previous sections to suppress the strength of vortex shedding in the critical regime.

Adding ribs with properties $h/d = 0.0067$ and $\Delta/h = 20$ yields Fig. 14. One can see from Fig. 14 that the trajectory of the C_D-Re curves for micro-roughness A ($S_A, h_{0.5}, \Delta_{10}$) and B ($S_B, h_{0.5}, \Delta_{10}$) are very similar besides a slightly lower Re_c for S_B, $h_{0.5}$, Δ_{10}. Increasing the micro-roughness further (S_C, $h_{0.5}$, Δ_{10}), decreases Re_c and increases $C_{D,min}$. St in Fig. 14 shows distinct peaks at the corresponding Re_c followed by a slow decrease for increasing Re, thus returning to the previously observed increase in shedding frequency at the critical Re.

These trends are roughly repeated for the various rib sizes and spacings (not shown), although for larger Δ/h and h/d the variation in St diminishes, in agreement with earlier observations. Interestingly, at the extreme of the parameter space where $h/d = 0.0267$ and $\Delta/h = 10$ (Fig. 15), one can see that the positive effect of the ribs more or less disappears and the different surface coatings only result in an increase in drag corresponding to the additional wetted area each of the surface coatings provide. For these cases of extreme roughness, the shedding frequency appears to be relative fixed for the tested Re, although they are likely all subcritical.

To summarise, increasing the surface micro-roughness generally decreases Re_c and increases $C_{D,min}$ as shown in Fig. 16. In the limit of large ribs and spacing, e.g., Fig. 15, the advantages of the surface coatings vanish and increasing the micro-roughness only results in increasing the total surface and thus skin friction. This, however, appears to be a

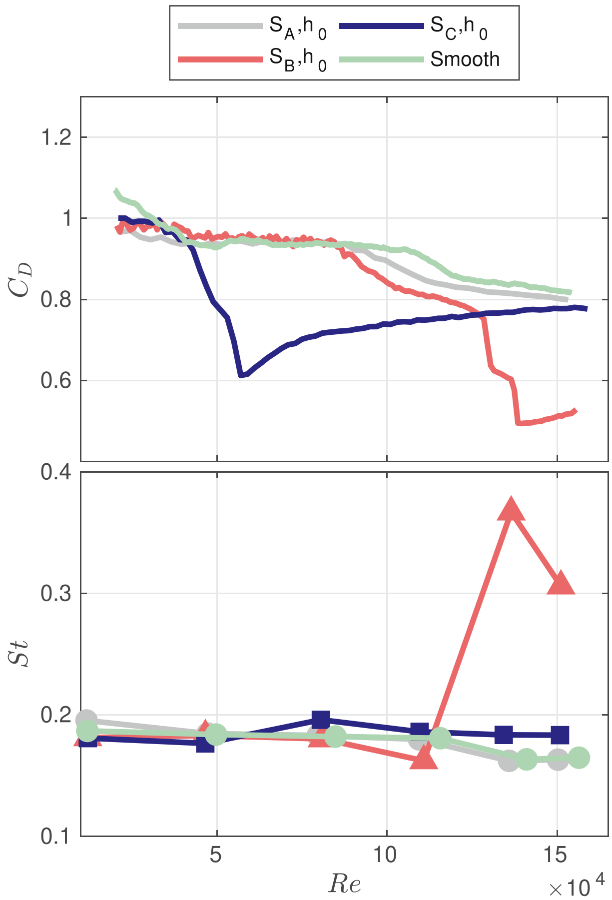

Fig. 13. Effect of varying the coating fabric for cylinders without ribs.

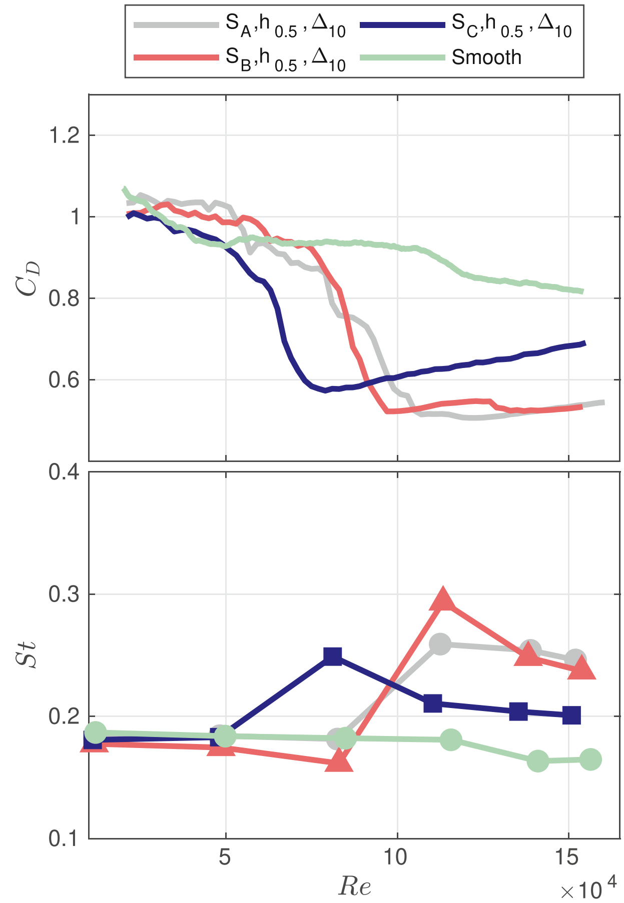

Fig. 14. Effect of varying the coating fabric for textiles with $h/d = 0.067$ and $\Delta/h = 20$.

consequence of the ribs rather than the micro-roughness.

4. Global results

Thus far, the results have been effectively binned into different categories for comparison, where only specific tests were investigated to address a particular question, e.g., what is the effect of rib spacing? In the present section, we consider the results of all tests together to make some global recommendations on what surface coatings create the greatest positive effects with respect to Re_c, $C_{D,min}$ and the average C_D over the measurement region.

4.1. Critical Reynolds number

In Fig. 17, Re_c is plotted against Δ/h for all test cases. In the figure, symbols are used to denote the different micro-roughnesses and the rib height and spacing increases with the darkness of the symbol. The lowest Re_c in this figure is approximately 25 000 for $\Delta/h = 5$ and coating S_A, h_2, Δ_{10}. However, S_C, h_2, Δ_{10} was not plotted due to its Re_c being below 20 000 and not measured; note that this is consistent with the observations in section 3.3 that micro-roughness C would produce a lower Re_c than micro-roughness A. S_A, h_2, Δ_{10} and S_C, h_2, Δ_{10} both have $\Delta/h = 5$, and the global trend visible in Fig. 17 suggests that this is the local minimum for all surface coatings. This relative spacing also gives the smallest spread between each surface coating. This result appears to be in agreement with those presented in section 3.1, which suggested an "optimal'' spacing existed to minimise Re_c. When all the evidence is considered as a whole, it suggests that this optimal spacing is near $\Delta/h = 5$ to minimise Re_c.

4.2. Minimum drag coefficient

The minimum drag coefficient for each surface coating, $C_{D,min}$, can also be plotted versus the relative rib spacing, Δ/h, as illustrated in Fig. 18. The surface coatings without ribs have been plotted as having $\Delta/h = 0$. Some of the surface coatings have not been plotted due to their drag crisis being outside of the measured Re range. Looking at those plotted in Fig. 18, S_B, h_0 yields the lowest $C_{D,min}$ of about 0.49. This is a surface coating without ribs, which indicates that ribs in general increase $C_{D,min}$. There are however some ribbed surface coatings that have nearly as low a value as S_B, h_0, e.g., $S_A, h_{0.5}, \Delta_{10}$ has a $C_{D,min} \approx 0.5$. As the smooth cylinder case did not yield a value inside the Re range, there is no base case value to compare with but generally it is known that it occurs at a much higher Re. However, a value of 0.5 is much larger than the smooth cylinder-value of 0.2, measured by Schewe (2001). This strengthens the argument that it is unlikely that the $C_{D,min}$ of a smooth cylinder can be replicated at lower Re. While it may not be possible to replicate the smooth cylinder $C_{D,min}$ at lower Re, it is still true that integrating the C_D over the range of Re investigated herein results in a lower value for many of the tested cases compared to the smooth case. Thus, for a body operating at low Re there may still be material benefits of using ribs and micro-roughness. This is investigated in the next sub-section.

4.3. Average drag coefficient

From an engineering standpoint, it is interesting to know which of the surface coatings minimises drag over a given range of velocities. It is therefore interesting to analyse the average C_D, $C_{D,avg}$, across different Re ranges rather than just a singular C_D at one Re. In Fig. 19, $C_{D,avg}$ for all

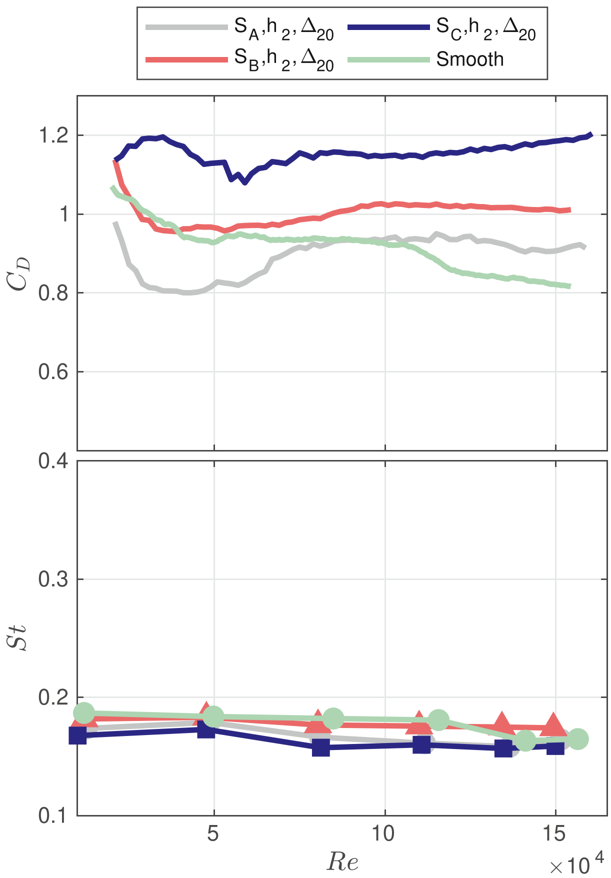

Fig. 15. Effect of varying the coating fabric for textiles with $h/d = 0.0267$ and $\Delta/h = 10$.

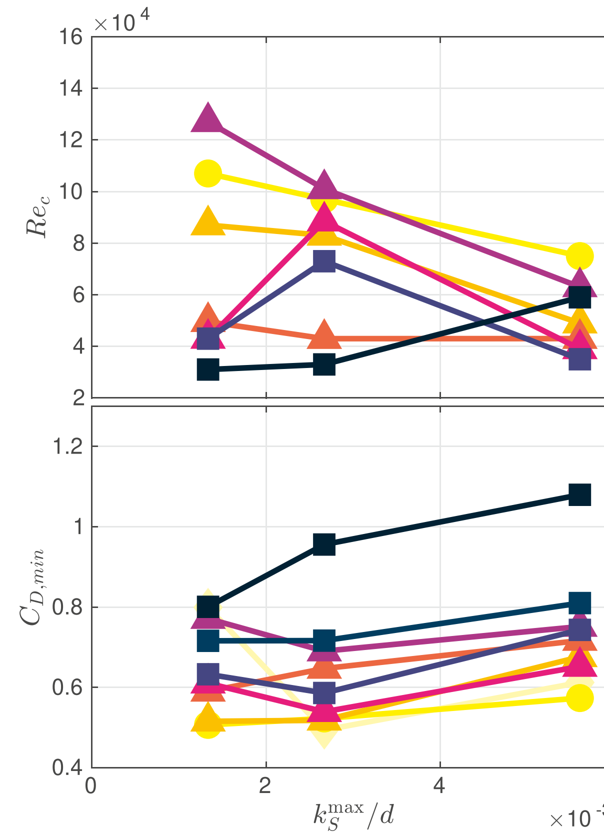

Fig. 16. The effect on Re_c and $C_{D,min}$ by varying the surface coating is plotted. The different curves have different relative rib height and rib spacing. Lines with circles have $h/d = 0.0067$, triangles have $h/d = 0.0133$ and squares have $h/d = 0.0267$. Darker colour means larger rib spacing. (For interpretation of the references to colour in this figure legend, the reader is referred to the Web version of this article.)

surface coatings, across the entire measured Re range, has been plotted. One can see that $C_{D,\text{avg}}$ across the measured Re range varies from 0.7 to 1.16 (66% change) for the tested surface coatings. For the smooth case, $C_{D,\text{avg}} \approx 0.9$, and many of the tested surface coatings lie below this, suggesting there is a benefit to employing them for this Re-range. The surface coatings with the lowest $C_{D,\text{avg}}$ are $S_A, h_1, \Delta_{2.5}$ (0.70), S_A, h_1, Δ_{10} (0.72) and S_A, h_1, Δ_5 (0.73). This means that choosing $S_A, h_1, \Delta_{2.5}$ instead of a smooth cylinder, gives an average drag reduction of approximately 22.6% for $Re < 160,000$. In addition to providing a drag reduction compared to the smooth cylinder, these surface coatings also have noticeably lower $C_{D,\text{avg}}$ than the coatings without ribs, S_A, h_0 (0.89), S_B, h_0 (0.84), S_C, h_0 (0.78). Thus, choosing the ribbed surface coating S_A, h_1, $\Delta_{2.5}$ instead of S_C, h_0 gives an average drag reduction of 9.6%.

Similar analysis can be performed for an infinite selection of Re-ranges. By selecting a few additional subranges, e.g., $20000 < Re < 90000$, $90000 < Re < 160000$, we observe that the specific values of the average C_D change with the Re-range, as one would expect, but that generally there are always ribbed surfaces that produce lower average C_D than a smooth cylinder or a cylinder with just micro-roughness. Furthermore, cylinders with $\Delta/h = 5$ and mild micro-roughness tend to robustly produce lower average drag, at least within the ranges investigated here.

5. Conclusions

The measurements performed and analysed in this work showed that adding spanwise ribs to the surface of a cylinder with a given micro-roughness can decrease both the C_D at a given Re and the $C_{D,\text{avg}}$ at any partition of the measured Re range investigated here. This is due to the effect the ribs have on the shape of the C_D-Re curve and the point of $C_{D,min}$

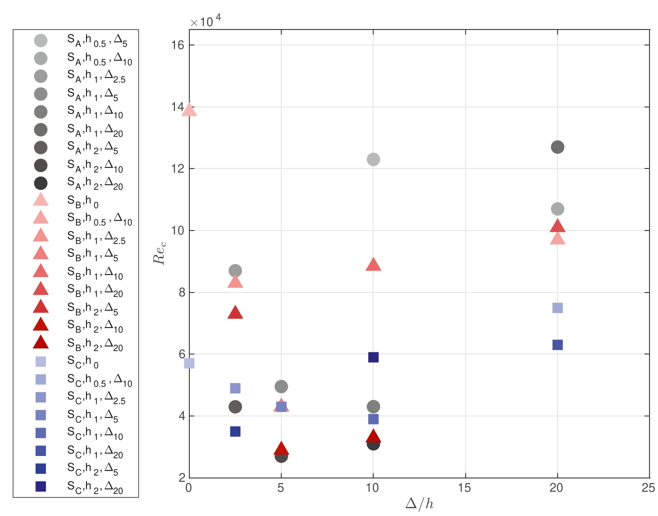

Fig. 17. Critical Reynolds number for all surface coatings plotted against their respective relative rib spacing, Δ/h.

and Re_c. The effect of the ribs on these properties was dependent on the rib size (h/d), the rib spacing (Δ/h) and the micro-roughness ($k_S^{\max}$). Increasing the rib size yielded higher $C_{D,min}$ and lower Re_c. It also decreased the frequency (St) at which vortices were shed at Re_c. The rib spacing had a different effect. An optimal rib spacing of $\Delta/h = 5$ caused the lowest Re_c, and from this point either increasing or decreasing the rib

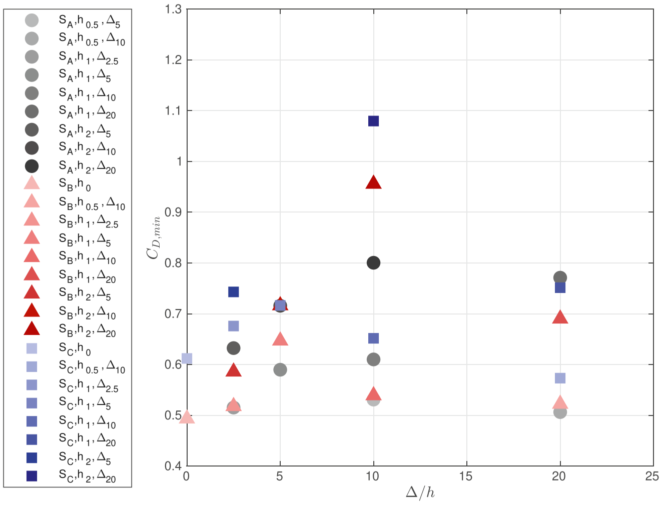

Fig. 18. Minimum drag coefficient for all surface coatings plotted against Δ/h.

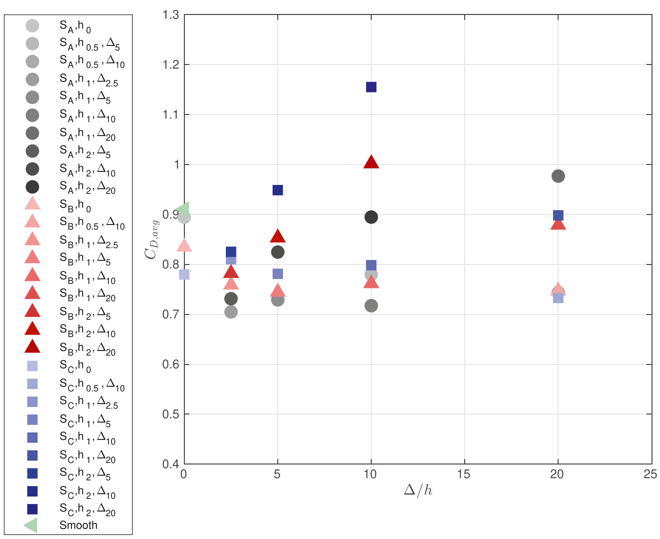

Fig. 19. Average C_D across the measured Re range ($20000 < Re < 160000$).

spacing caused an increase in Re_c. The smallest rib spacing gave the lowest $C_{D,min}$ and by increasing the rib spacing, the $C_{D,min}$ was increased. When micro-roughness was added at increasing levels to the ribbed cylinder, the general trend showed that the Re_c decreased and $C_{D,min}$ increased. This is consistent with the view that larger micro-roughness increases the skin friction.

By taking the average of C_D throughout the measured Re range ($20,000 < Re < 160,000$), the average drag savings by choosing ribbed surface coatings instead of a smooth surface was found. The maximum savings in average drag was found to be 22.6% for choosing textile $S_A, h_1, \Delta_{2.5}$; this is a surface coating with relative rib height $h/d = 0.0133$, relative rib spacing $\Delta/h = 2.5$, and maximum relative micro-roughness height of $k_S^{max}/d = 0.0013$. Thus, considering all facets investigated herein, for the investigated Re range, $S_A, h_1, \Delta_{2.5}$ produced the minimum drag over the tested range. Nonetheless, it is important to understand the limitation that at higher Re, none of the presented surface coatings would improve upon the drag of a smooth cylinder, and thus these benefits are limited to the low Re range.

Declaration of competing interest

The authors declare that they have no known competing financial interests or personal relationships that could have appeared to influence the work reported in this paper.

CRediT authorship contribution statement

Arne Kilvik Skeide: Data curation, Formal analysis, Investigation, Methodology, Writing - original draft. **Lars Morten Bardal:** Methodology, Data curation. **Luca Oggiano:** Conceptualization. **R. Jason Hearst:** Conceptualization, Methodology, Supervision, Writing - original draft, Writing - review & editing.

Acknowledgements

RJH is financially supported by the Research Council of Norway (project no. 288046).

References

Achenbach, Elmar, 1971. Influence of surface roughness on the cross-flow around a circular cylinder. J. Fluid Mech. 46 (2), 321–335.
Ahmed, Anwar, Bays-Muchmore, Byram, 1992. Transverse flow over a wavy cylinder. Phys. Fluid. Fluid Dynam. 4 (9), 1959–1967.
Anderson, John D., 2017. Fundamentals of Aerodynamics, sixth ed. McGraw-Hill Education.
Bearman, P.W., Harvey, J.K., 1993. Control of circular cylinder flow by the use of dimples. AIAA J. 31 (10), 1753–1756.
Brownlie, Leonard William, 1992. Aerodynamic Characteristics of Sports Apparel. PhD thesis, Theses. School of Kinesiology)/Simon Fraser University.
Cengel, Yunus A., Cimbala, John M., 2014. Fluid Mechanics: Fundamentals and Applications, third ed. The McGraw-Hill Companies.
Flack, K.A., 2018. Moving beyond Moody. J. Fluid Mech. 842, 1–4.
Flack, K.A., Schultz, M.P., 2010. Review of hydraulic roughness scales in the fully rough regime. J. Fluid Eng. 132, 041203.
Schewe, Günter, 2001. Reynolds-number effects in flow around more-or-less bluff bodies. J. Wind Eng. Ind. Aerod. 89 (14–15), 1267–1289.
Hsu, X.Y., Miau, J.J., Tsai, J.H., Tsai, Z.X., Lai, Y.H., Ciou, Y.S., Shen, P.T., Chuang, P.C., Wu, C.M., 2019. The aerodynamic roughness of textile materials. J. Textil. Inst. 110 (5), 771–779.
Hwang, Jong-Yeon, Yang, Kyung-Soo, 2007. Drag reduction on a circular cylinder using dual detached splitter plates. J. Wind Eng. Ind. Aerod. 95 (7), 551–564.
Kimura, Takeyoshi, Tsutahara, Michihisa, 1991. Fluid dynamic effects of grooves on circular cylinder surface. AIAA J. 29 (12), 2062–2068.
Ko, N.W.M., Leung, Y.C., Chen, J.J.J., 1987. Flow past v-groove circular cylinders. AIAA J. 25 (6), 806–811.
Lam, K., Lin, Y.F., 2009. Effects of wavelength and amplitude of a wavy cylinder in cross-flow at low Reynolds numbers. J. Fluid Mech. 620, 195–220.
Lee, Sang-Joon, Kim, Hyoung-Bum, 1997. The effect of surface protrusions on the near wake of a circular cylinder. J. Wind Eng. Ind. Aerod. 69, 351–361.
Lim, Hee-Chang, Lee, Sang-Joon, 2002. Flow control of circular cylinders with longitudinal grooved surfaces. AIAA J. 40 (10), 2027–2036.
Hultmark, Marcus, Smits, Alexander J., 2010. Temperature corrections for constant temperature and constant current hot-wire anemometers. Meas. Sci. Technol. 21 (10), 105404.
Matsumura, Toshio, Yura, Toshiki, Kikuchi, Naoshi, Matsumoto, Tetsuo, Takeuchi, Hitoshi, Iwasaki, Kunio, Tominaga, Yasuhiro, 2002. Development of low wind-pressure insulated wires. Furukawa Electr. Rev. 39–44.
Nakamura, Yo, Tomonari, Y., 1982. The effects of surface roughness on the flow past circular cylinders at high Reynolds numbers. J. Fluid Mech. 123, 363–378.
Nebres, J., Batill, S., 1993. Flow about a circular cylinder with a single large-scale surface perturbation. Exp. Fluid 15, 369–379.
Oggiano, Luca, Brownlie, Len, Troynikov, Olga, Bardal, Lars Morten, Sæter, Camilla, Sætran, Lars, 2013. A review on skin suits and sport garment aerodynamics: guidelines and state of the art. Procedia Eng. 60, 91–98.
Roshko, Anatol, 1961. Experiments on the flow past a circular cylinder at very high Reynolds number. J. Fluid Mech. 10 (3), 345–356.
Schewe, G., 1983. On the force fluctuations acting on a circular cylinder in crossflow from subcritical up to transcritical Reynolds numbers. J. Fluid Mech. 133, 265–285.
Walsh, M.J., Weinstein, L.M., 1979. Drag and heat-transfer characteristics of small longitudinally ribbed surfaces. AIAA J. 17 (7), 770–771.
West, G.S., Apelt, C.J., 1982. The effects of tunnel blockage and aspect ratio on the mean flow past a circular cylinder with Reynolds numbers between 10^4 and 10^5. J. Fluid Mech. 114, 361–377.
Yamagishi, Yoichi, Oki, Makoto, 2004. Effect of groove shape on flow characteristics around a circular cylinder with grooves. J. Visual 7 (3), 209–216.

Yamagishi, Yoichi, Oki, Makoto, 2005. Effect of the number of grooves on flow characteristics around a circular cylinder with triangular grooves. J. Visual 8 (1), 57–64.

Zdravkovich, M.M., 1981. Review and classification of various aerodynamic and hydrodynamic means for suppressing vortex shedding. J. Wind Eng. Ind. Aerod. 7 (2), 145–189.

Zhang, Kai, Katsuchi, Hiroshi, Zhou, Dai, Yamada, Hitoshi, Han, Zhaolong, 2016. Numerical study on the effect of shape modification to the flow around circular cylinders. J. Wind Eng. Ind. Aerod. 152, 23–40.

Zhou, T., Mohd Razali, S.F., Hao, Z., Cheng, L., 2011. On the study of vortex-induced vibration of a cylinder with helical strakes. J. Fluid Struct. 27 (7), 903–917.